

## Article

# Reduction of an Ilmenite Concentrate by Using a Novel CO<sub>2</sub>/CH<sub>4</sub> Thermal Plasma Torch

Mohammed El Khalloufi <sup>1</sup>, Gervais Soucy <sup>1,\*</sup>, Jonathan Lapointe <sup>2</sup> and Mathieu Paquet <sup>2</sup>

<sup>1</sup> Département de Génie Chimique et de Génie Biotechnologique, Université de Sherbrooke, Sherbrooke, QC J1K 2R1, Canada; mohammed.el.khalloufi@usherbrooke.ca

<sup>2</sup> Ressources Metchib Inc., 756 4e Rue, Chibougamau, QC G8P 1S5, Canada; jonathan.lapointe@metchib.com (J.L.); mathieu.paquet@metchib.com (M.P.)

\* Correspondence: gervais.soucy@usherbrooke.ca; Tel.: +1-819-821-8000 (ext. 62167)

**Abstract:** Plasma technology has emerged as a very helpful tool in a variety of sectors, notably metallurgy. Innovators and scientists are focused on the problem of finding a more ecologically friendly way of extracting titanium and iron metal from natural ilmenite concentrate for industrial applications. A direct current (DC) plasma torch operating at atmospheric pressure is used in this study to describe a decarbonization process for reducing an ilmenite concentrate. The plasma gases employed in this torch are CO<sub>2</sub> and CH<sub>4</sub>. The molar ratio of the gases may be crucial for achieving a satisfactory reduction of the ilmenite concentrate. As a result, two molar ratios for CO<sub>2</sub>/CH<sub>4</sub> have been chosen: 1:1 and 2:1. During torch operation, a thin layer of graphite is formed on the cathode to establish a protective barrier, prolonging the cathode's life. The material was analyzed using X-ray diffraction (XRD) and scanning electron microscopy with energy dispersive spectroscopy (SEM-EDS). The output gases were analyzed using mass spectrometry (MS). In addition, a thermodynamic analysis was performed to predict the development of thermodynamically stable phases. An economic assessment (including capital expenditures (CAPEX) and operating expenditures (OPEX)) and a carbon balance were developed with the feasibility of the piloting in mind.

**Keywords:** plasma technology; metallurgy; ilmenite concentrate; titanium; iron metal; reduction; CO<sub>2</sub>/CH<sub>4</sub> plasma torch



**Citation:** El Khalloufi, M.; Soucy, G.; Lapointe, J.; Paquet, M. Reduction of an Ilmenite Concentrate by Using a Novel CO<sub>2</sub>/CH<sub>4</sub> Thermal Plasma Torch. *Minerals* **2024**, *14*, 502. <https://doi.org/10.3390/min14050502>

Academic Editors: Lei Gao, Bangfu Huang, Fan Zhang and Guo Chen

Received: 27 March 2024

Revised: 7 May 2024

Accepted: 8 May 2024

Published: 10 May 2024



**Copyright:** © 2024 by the authors. Licensee MDPI, Basel, Switzerland. This article is an open access article distributed under the terms and conditions of the Creative Commons Attribution (CC BY) license (<https://creativecommons.org/licenses/by/4.0/>).

## 1. Introduction

Thermal plasma is being used more and more to get back metals, complex compounds, and minerals such as ilmenite that have been lost. This technology has shown a high reduction power for a variety of minerals containing multiphases that are extremely difficult to separate [1]. As a result, thermal plasma is distinguished by high temperatures that reach 20,000 K and high electron density, which makes the plasma arc more stable. One of the most well-known properties of thermal plasmas is local thermal equilibrium (LTE) [2].

Plasma processing has enormous potential in a variety of fields (aerospace, transportation, biomedical, and military), where the demand for materials with significantly improved physical and mechanical properties is increasing. Plasma processing offers unrivaled benefits in extractive metallurgy. It allows for the formation of reactive plasma species at high temperatures, which may speed up the chemical reactions. Furthermore, the residence time is short and controllable [2]. Thermal plasmas provide a variety of options for decarbonizing industrial processes by decreasing greenhouse gas emissions, treating hazardous waste more cleanly, generating energy from renewable sources, and improving industrial process efficiency while lowering their carbon footprint [3].

Scientists have tried several techniques for producing newer and better materials for several decades; however, plasma technology has emerged and developed to replace traditional methods of producing high-quality materials and purifying metals at a low cost with high productivity. Plasma, as previously defined, is a physical state with high

electrical conductivity and gaseous properties. A plasma arc can be created by passing a current through a gas [4]. Consequently, when electrons are accelerated in a gaseous medium, thermal plasma forms between two electrodes. As a result, the electron speed can cause collisions between electrons and charged particles, resulting in kinetic energy transfer and increasing the temperature of the gas [4].

Ilmenite is a type of ore that contains more than 40 wt.% TiO<sub>2</sub> [5]. Titanium and iron are critical metals in many industries, including the aerospace, automotive, and chemical industries, and the military [6]. Titanium's great strength, low density, biocompatibility, and corrosion resistance have made it a popular material [7]. However, titanium's strong affinity for oxygen results in high manufacturing costs and poor productivity; therefore, the metal is mostly used for specialized applications [8].

The most well-known industrial technique for producing pure titanium is the Kroll process. This method is based on the magnesiothermic reduction of titanium tetrachloride TiCl<sub>4</sub>. The feed material is TiO<sub>2</sub> or UGS (upgraded slag containing approximately 95 wt.% TiO<sub>2</sub>), which is carbochlorinated at 1000 °C to produce purified TiCl<sub>4</sub>. Magnesium reduces synthetic TiCl<sub>4</sub> at 800 °C to produce titanium. Vacuum distillation is used to remove byproducts and unwanted products. On the other hand, the Kroll process is still a low-productivity, high-cost titanium production technique, and is not an environment-friendly process [9].

For decades, scientists have developed numerous techniques to replace the Kroll process and lower the cost of titanium primary metal [10]. The Armstrong process, which is similar to the Hunter process, is one of the modified processes. The TiRO process is a new procedure developed by Australia's Commonwealth Scientific and Industrial Research Organization (CSIRO). It uses the same chemistry as the Kroll process in a continuous manner [11]. Some of the electrochemical methods developed to produce titanium at a low cost include the Ono and Suzuki (OS) process [12], the Fray-Farthing-Chen (FFC) Cambridge process [13], and the Electronically Mediated Reduction (EMR) process [14]. A review paper that summarizes all metallurgical extraction methods for titanium from its concentrations has already been published [5].

Numerous studies have explored the reduction of ilmenite concentrate using thermal plasma technology to produce various essential products for diverse applications. For example, research investigated the production of fine titanium carbide powder by employing ilmenite concentrate and methane as feed in a thermal plasma reactor [15]. Another study examined the thermal decomposition of ilmenite concentrates in a non-transferred arc thermal plasma flow reactor, where the plasma torch operated with argon-helium and argon-nitrogen mixtures as plasma gases [16]. Additionally, successful processing of pre-reduced ilmenite concentrate from the Indian region was achieved using thermal plasma methods to yield high titania slag. This study investigated the effects of various factors, including time, yield, and energy consumption, on the concentrations of TiO<sub>2</sub> and FeO in the slag [17]. Furthermore, the synthesis of TiO<sub>2</sub> nanoparticles was conducted in a non-transferred arc thermal plasma reactor using ilmenite as the precursor material [18].

The DC plasma torch, developed at the Centre for Advanced Coating Technologies (CACT) at the University of Toronto primarily for thermal spraying, utilizes molecular gases for plasma generation. In contrast to commercial torches that rely on argon or air as plasma-forming gases, this torch employs a mixture of CO<sub>2</sub> and CH<sub>4</sub> (or any other hydrocarbon). One drawback of using argon as a plasma gas is its low thermal conductivity, which diminishes the heat transfer rate to the treated materials. To address this limitation, small percentages of hydrogen or helium are typically added [19]. While this addition enhances heat transfer, it also accelerates electrode erosion. During arc combustion, the hydrocarbons undergo complete dissociation into free carbon and hydrogen. Under appropriate conditions, carbon ions from the gas phase diffuse to the cathode surface, establishing a dynamic equilibrium between carbon sublimation and precipitation. CO<sub>2</sub>-CH<sub>4</sub> plasmas are technologically desirable in materials processing because they have a greater enthalpy

at lower temperatures. For example, at 7000 K, it has an enthalpy of over 50 MJ/kg, as compared to 20 MJ/kg for argon plasma [20].

In comparison investigations of the same torch operating with Ar-CH<sub>4</sub> and CO<sub>2</sub>-CH<sub>4</sub> under similar input parameters (such as current and total gas flow rate), it was discovered that the arc voltages were higher when utilizing the CO<sub>2</sub>-containing mixture. At a current of about 340 A, the arc voltage reached 140 V, indicating a considerable, nearly twice-doubling increase in the torch’s thermal efficiency [21]. Notably, the formation of positive carbon ions within the arc causes an ionic current to flow towards the cathode, where carbon ions are deposited on its surface. This phenomenon of carbon ion deposition is rapid, forming a disc-shaped deposit ranging from 3 to 6 mm in diameter within a matter of seconds at the arc attachment point [22].

This study describes a novel method for reducing an ilmenite concentrate using a direct current torch. CO<sub>2</sub> and CH<sub>4</sub> are the plasma gases used in this study. Two CO<sub>2</sub>/CH<sub>4</sub> molar ratios have been used: 1:1 and 2:1, which may result in a good reduction environment inside the reactor. The impact of the CO<sub>2</sub>/CH<sub>4</sub> molar ratio was investigated, and it was shown that a 1:1 ratio produced greater temperatures and power within the reactor than a 2:1 molar ratio, resulting in a more effective reduction of the ilmenite concentrate. The results show that by using thermal plasma treatment, the ilmenite concentrate was partially reduced, and titanium and iron metal might be produced in the cone part where the temperature could reach a high level. As a result, plasma treatment could be used as a novel method to produce some pure metals.

## 2. Materials and Methods

### 2.1. Chemicals

In the torch plasma experiment, pure CO<sub>2</sub> (99 wt.%) and CH<sub>4</sub> (99 wt.%) gases are used, and pure argon gas (99 wt.%) is used to cool the experiment. Metchib Company, Quebec, Canada, provided an ilmenite concentrate. The elemental composition of the ilmenite concentrate is presented in Table 1, while the particle size distribution is illustrated in Figure 1. The plasma torch was supplied by two types of CO<sub>2</sub>/CH<sub>4</sub> molar gas ratios: 1:1 and 2:1.

**Table 1.** Elemental composition of the ilmenite concentrate (unit: wt.%).

	Fe <sub>2</sub> O <sub>3</sub>	TiO <sub>2</sub>	SiO <sub>2</sub>	Al <sub>2</sub> O <sub>3</sub>	CaO	Mn <sub>3</sub> O <sub>4</sub>	MgO	V <sub>2</sub> O <sub>5</sub>	LOI
Ilmenite concentrate	45.50	37.15	3.84	2.15	1.29	0.75	0.41	0.29	3.93

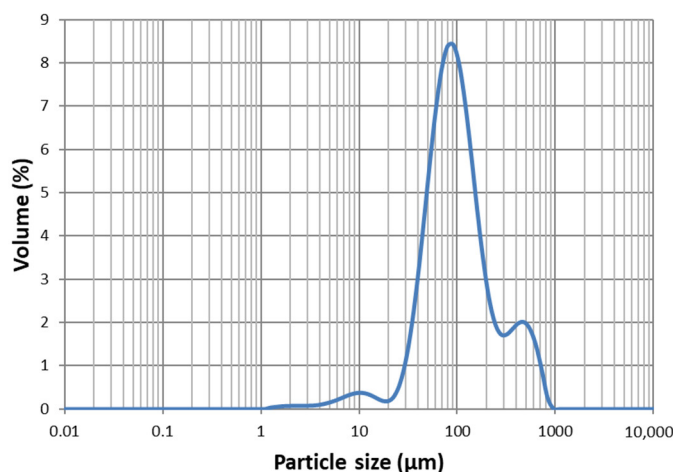


**Figure 1.** Particle size distribution of ilmenite concentrate.

## 2.2. Experimental Procedure

With a mixture of CO<sub>2</sub> and hydrocarbon (CH<sub>4</sub>) gas, a new direct current (DC) plasma torch has been used to reduce an ilmenite concentrate. Compared to traditional DC thermal plasma torches, this new torch has better plasma enthalpy, better thermal conductivity, a working gas (CO<sub>2</sub>) that is easy to get, and a long electrode life [20]. A spouted bed reactor has been designed for reducing an ilmenite concentrate. This device demonstrated its efficiency by reaching extremely high temperatures while minimizing the partial pressure of oxygen inside the reactor. The ilmenite concentrate was thermally treated by the plasma torch in the following manner: 250 g of an ilmenite concentrate was used to feed the experiments. The CO<sub>2</sub> and CH<sub>4</sub> plasma gases were put into the torch's discharge zone at a controlled rate. Time zero ( $t = 0$ ) was established as the moment when plasma ignition began. CO<sub>2</sub> and CH<sub>4</sub> are two greenhouse gases that are used to create a stable plasma arc with a high enthalpy (50 MJ/kg) and thermal conductivity ( $\approx 4$  W/m.K) [20]. At high temperatures, the CO<sub>2</sub>/CH<sub>4</sub> mixture has a complex composition in which a CO presence could occur and reduce oxidation. A fine layer of graphite was deposited on the cathode, extending its lifetime. To create a reduced environment, the molar gas ratio was set to 1:1 and then 2:1, the torch current was constant at 252 A, and the voltage was adjusted to 155 V, while the pressure neared 1 atm. The material was heated until the region nearest to the torch became red. The experiment was limited to 3 min due to the overheating of the conical part and the production of hot spots, which might cause damage to the plasma reactor. Figure 2 depicts the experimental setup.

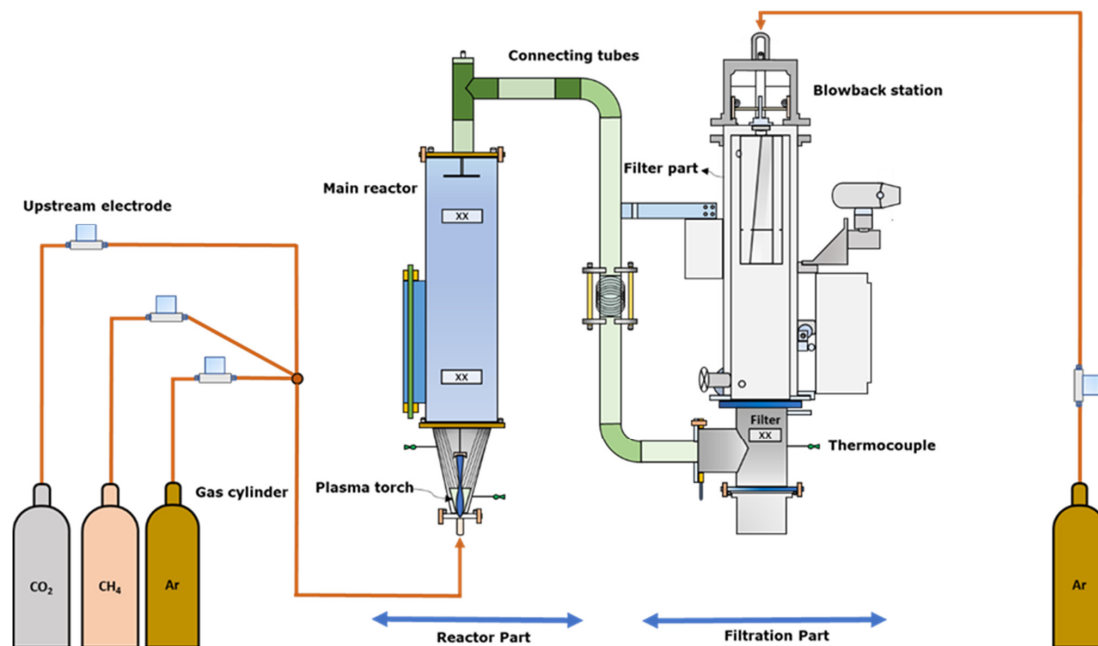


**Figure 2.** The experimental setup.

## 2.3. Characterization Techniques

### 2.3.1. Particle Size Analysis

A SYNC particle analyzer was used to determine the particle size distribution of ilmenite concentrate. Microtrac's SYNC particle analyzer (Microtrac Retsch GmbH, Haan/Duesseldorf, Germany) represents a significant advance in the characterization of materials in terms of particle size. This advanced system incorporates Microtrac's tri-laser diffraction technology, renowned for its accuracy and reliability in determining particle size. The SYNC analyzer offers exceptional measurement capability over a wide range of particle sizes. Lasers of different wavelengths enable enhanced resolution, effectively covering particles of different sizes, from nanometers to micrometers (10 nm to 4 mm).

### 2.3.2. XRF Analysis

The Panalytical Axios Advanced spectrometer (Malvern Panalytical, Westborough, MA, USA) is a wavelength-dispersive X-ray fluorescence (WD-XRF) analysis instrument. It was used to determine the elemental composition and mass concentrations of the raw material. Using wavelength dispersion technology, the Axios Advanced spectrometer excels in its ability to probe the chemical composition of materials. Exposing the sample to X-rays causes the emission of characteristic fluorescent X-rays, whose energies and intensities are measured with extreme precision. This approach enables reliable identification of the elements present, from major components to minute traces. The standard limit of detection (LOD) for quantitative analysis is approximately 0.01%. A loss on ignition (LOI) step is required for XRF analysis. The maximum temperature for the loss on ignition is 1050 °C.

### 2.3.3. XRD Analysis

The Panalytical Company's X'Pert Pro MPD diffractometer (Malvern Panalytical, Westborough, MA, USA) was used to identify all the present phases before and after plasma treatment. The starting angle is 10° and the ending angle is 70°, with a step of 1°/min, using Cu  $\alpha$  radiation. Rietveld analyses were performed using HighScore Plus version 4.9 to determine the fraction of phases in the samples. High sample crystallinity is required for proper analysis. This approach has a remarkable limit of detection (LOD) of 0.2 wt.%, a limit of quantification (LOQ) below 1 wt.%, and good accuracy for quantifying phase proportions [23]. In this work, Rietveld analysis was performed by assigning peaks to the crystalline phases seen on XRD diagrams, and the simulation parameters were improved until the estimated error was less than 2 wt.% [24]. Results indicated that quantification was generally more accurate when background noise was not refined, despite higher concordance indices. Reducing the number of refined parameters also simplified refinement and provided a more precise assessment of model quality. Values below 10 were anticipated for Rwp and below 4 for GOF (goodness of fit). GOF values are heavily influenced by the number of refined parameters and, consequently, are not considered highly reliable. Overall, visual inspection combined with concordance index values allows for a robust model evaluation. For all refinement tests, a pseudo-Voigt profile function and the Newton-Raphson nonlinear least squares fitting method were employed.

### 2.3.4. SEM-EDS Analysis

The microstructural analysis was performed using a Hitachi S-4700 microscope (Hitachi, Ltd., Tokyo, Japan). EDS analyzed the morphology of samples to determine the elemental composition of the material. The advanced technology of the Hitachi S-4700 scanning electron microscope allows for high-resolution pictures to be acquired from a broad range of materials. EDS examined the microstructure of materials to identify their elemental composition. The resolution of EDS analysis is high, and only elements with a concentration of less than 0.01% cannot be detected by this technique. Light elements cannot be detected using EDS.

### 2.3.5. MS Analysis

Cirrus 2 (MKS Instruments UK Ltd., Cheshire, UK) carries out gas analysis at the reactor outlet. The latter is a benchtop quadrupole mass spectrometer specially designed for monitoring gases at atmospheric pressure. Incorporating the latest Cirrus 2 hardware, the Cirrus 2 has been designed to meet all the traditional requirements of a laboratory sensor while offering data collection speeds in the millisecond range. The mass-spectrometric procedure involves the ionization of gas molecules within the spectrometer. Once ionized, the molecules are separated based on their mass-to-charge ratio ( $m/z$ ) by the quadrupole mass analyzer. The resulting mass spectrum provides information about the composition and concentration of gases present in the sample. The method's limit of detection (LOD) ranges approximately around  $1.33 \times 10^{-8}$  mbar, with a limit of quantification (LOQ) of about  $4 \times 10^{-8}$  mbar.

#### 2.4. Thermodynamic Study

The main goal of the thermodynamic calculations is to predict which phases will form after plasma treatment of ilmenite. As a result, the effect of the CO<sub>2</sub>/CH<sub>4</sub> molar ratio on the reduction of ilmenite concentrate was investigated. The mixture composition of the reaction between CO<sub>2</sub> and CH<sub>4</sub> has been calculated at atmospheric pressure and temperatures ranging from 25 °C to 5000 °C, using molar ratios of 1:1 and 2:1. Similarly, the reaction composition of the torch exit gases and ilmenite phase FeTiO<sub>3</sub> was calculated. As a result, the pressure remains constant at 1 atm, but the temperature varies from 500 °C to 3000 °C. All thermodynamic calculations were performed using Factsage software, version 8.3. It is based on the principle of optimizing the Gibbs free energy of all thermodynamic reactions involving selected chemical species. It consists of a nonlinear program that uses the concept of the penalty function to deal directly with equality and inequality constraints. These constraint problems were solved using the modified Newton technique, as described by Lantagne, G. [25]. The minimization equations are developed using Sandler's approach, as shown by Lantagne, G. [25]. The notation for this function is as follows:

$$G = \sum_{j=0}^M G_j^0 n_j + \sum_{i=0}^n n_i (G_i^0 + RT \ln \frac{n_i}{n_T} + RT \ln \frac{P}{P_{ref}}) \quad (1)$$

where  $M$  is the number of compounds present as condensed phases,  $n$  is the number of species in the gas phase,  $n_i$  is the number of moles of species  $i$ ,  $n_j$  is the number of moles of species  $j$ ,  $G_i$  is the Gibbs free energy of species  $i$  in its reference state,  $G_j$  is the Gibbs free energy of species  $j$  in its reference state,  $R$  is the perfect gas constant,  $T$  is the system temperature,  $P$  is the system pressure, and  $P_{ref}$  is the reference pressure.

Minimizing the free energy of the mixture is constrained by the conservation equation for each atomic element:

$$\sum_{k=0}^n a_{p,k} N_k = b_p \quad (2)$$

where  $a_{p,k}$  is the number of atom  $p$  in species  $k$  and  $b_p$  is the total number of atomic element  $p$  in the system.

To calculate the equilibrium of a realistic system, all chemical species must be included while calculating concentrations. The study of an overall reaction system requires the gathering of data on a diverse set of chemical species. However, in the event of complicated families of chemicals, the researcher must first assess the stability of each species before incorporating them. When concentrations are calculated for a small number of chemicals, or when thermodynamically stable chemical species are eliminated, we refer to a limited equilibrium, in which the mixture reaches a pseudo-equilibrium state that can persist for a while [26].

Two different reaction processes were investigated when reducing ilmenite concentrate. The first is a reaction between CO<sub>2</sub> and CH<sub>4</sub> inside the plasma torch, whereas the second is a reaction between the torch exit gases and the ilmenite phase. Table 2 shows the gas composition at the torch outlet for the two molar ratios (1:1 and 2:1). Seventy-one species were chosen to cover the liquid, solid, and gas species formed from the entire reaction of the plasma gas combination CO<sub>2</sub>/CH<sub>4</sub> at molar ratios of 1:1 and 2:1, and the database FactPS (Fact pure substance database) was used for these calculations. Similarly, 131 species were selected to represent all gaseous, liquid, and solid phases, and 181 species and 29 solutions were included in the calculation to account for all potential solutions created during the equilibrium between the torch exit gases and FeTiO<sub>3</sub>. The following three databases were chosen: FactPS (fact pure substance database), FToxid (oxide database for slags, glasses, ceramics, and refractories), and Fstel (steel database). The plots highlight the species with a high mass fraction. To represent the results, only species with log<sub>10</sub> (mass fraction) ≥ −8 are shown on the graph.

**Table 2.** The gas composition at the torch output for the two molar ratios 1:1 and 2:1.

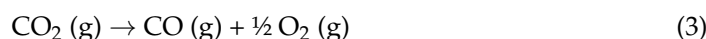
	Torch Output (%)						
	H <sub>2</sub>	CO	CH <sub>4</sub>	CO <sub>2</sub>	C <sub>2</sub> H <sub>2</sub>	H <sub>2</sub> O	O <sub>2</sub>
Ratio 1:1	1.4	21.7	11.7	32.7	19.1	13.2	0.2
Ratio 2:1	1.3	18.5	10.6	42.3	8.3	18.4	0.6

### 3. Results and Discussion

#### 3.1. Thermodynamic Study

##### 3.1.1. CO<sub>2</sub>/CH<sub>4</sub> Molar Ratio 1:1

The CO<sub>2</sub>/CH<sub>4</sub> mixture's chemical equilibrium has been calculated. CO<sub>2</sub> is an oxidative agent, which can result from the following decomposition reaction [27]:



The presence of CH<sub>4</sub> in the plasma gas mixture causes the deposition of a stream of positive carbon ions on the negatively charged cathode's surface. This carbon deposit protects the electrode from erosion and extends its life [27]. The reaction between CO<sub>2</sub> and CH<sub>4</sub> can generate carbon monoxide (CO) and hydrogen (H<sub>2</sub>) as soon as the temperature rises. Above 3000 °C, H<sub>2</sub> begins to decrease, but CO remains stable up to 5000 °C. The dissociation of CH<sub>4</sub> into acetylene (C<sub>2</sub>H<sub>2</sub>) and hydrogen (H<sub>2</sub>) is another chemical reaction that may occur under certain conditions:



Carbonyl (H<sub>2</sub>CO) and methyl (CH<sub>3</sub>) radicals are formed mainly from CO<sub>2</sub> and CH<sub>4</sub> molecules, respectively, after activation. When the methyl and carbonyl radicals react, they give rise to methanol, which then decomposes into carbon monoxide and the methyl radical. The latter, in turn, reacts with a second CH<sub>4</sub> molecule, producing hydrogen and carbon monoxide. The result of this complex chemical reaction is the production of CO and H<sub>2</sub> from CO<sub>2</sub> and CH<sub>4</sub> at high temperatures. When the temperature drops below the point where continuing the reaction is no longer energetically advantageous, the concentration of reactants decreases, and the process repeats itself. In conclusion, radicals and other intermediates are produced during the high-temperature reaction of CO<sub>2</sub> and CH<sub>4</sub>, which then undergo further reactions to yield CO and H<sub>2</sub> [28]. The variation of the mass fraction of the chemical species produced from the CO<sub>2</sub>/CH<sub>4</sub> gas plasma mixture as a function of temperature is illustrated in Figure 3.

Thermodynamic equilibria of the CO<sub>2</sub>/CH<sub>4</sub> plasma mixture with a molar ratio (1:1) for the CO<sub>2</sub>-CH<sub>4</sub> plasma mixture and FeTiO<sub>3</sub> system were investigated. As shown in Figure 3, the reaction between CO<sub>2</sub> and CH<sub>4</sub> by varying the temperature up to 5000 °C under atmospheric pressure produced different gaseous species. Furthermore, C<sup>+</sup> formation was discovered at around 3000 °C, allowing for cathode protection and extending its lifetime [29]. The CO<sub>2</sub> and CH<sub>4</sub> levels decreased during the reaction, resulting in more H<sub>2</sub> and CO and making the medium more reductive [30]; furthermore, increasing the temperature reduced the amount of water vapor produced because the ratio (1:1) does not favor the production of H<sub>2</sub>O [31]. The mass fraction variation of the predicted species for the reaction between the plasma CO<sub>2</sub>/CH<sub>4</sub> mixture at the torch output and ilmenite FeTiO<sub>3</sub> at atmospheric pressure is shown in Figure 4. The ilmenite phase (FeTiO<sub>3</sub>) and pseudobrookite (FeTi<sub>2</sub>O<sub>5</sub>) are stable, although their mass fraction decreases with increasing temperature. Furthermore, TiO<sub>2</sub> is formed at low temperatures, and its mass fraction stays constant when temperatures rise below 3000 °C. Ti<sub>2</sub>O<sub>3</sub> and Fe<sub>2</sub>O<sub>3</sub> are also produced at low temperatures, and their mass fractions increase with increasing temperature. Iron metal Fe(s) is produced at roughly 500 °C, followed by liquid phase Fe(liq), which is stable until 3000 °C. The CO<sub>2</sub>/CH<sub>4</sub> plasma torch may reduce the ilmenite concentrate in a series of

stages. The sequence seen is:  $\text{FeTiO}_3 \rightarrow \text{FeTi}_2\text{O}_5 \rightarrow \text{Ti}_2\text{O}_3 \rightarrow \text{TiO}_2 + \text{Fe}$  [32]. At 1000 °C, titanium’s solid and liquid phases appear, and their mass fractions increase until 3000 °C.  $\text{TiO}_2(\text{g})$ ,  $\text{TiO}(\text{g})$ , and  $\text{Ti}(\text{g})$  evolved at temperatures of around 1200 °C, 1400 °C, and 1600 °C, respectively. The reaction mechanism of ilmenite in a plasma mixture at high temperatures comprises, in brief, the dissociation of the mineral into its component elements, which may then react with other species in the plasma to generate different metallic and metallic oxide products [33].

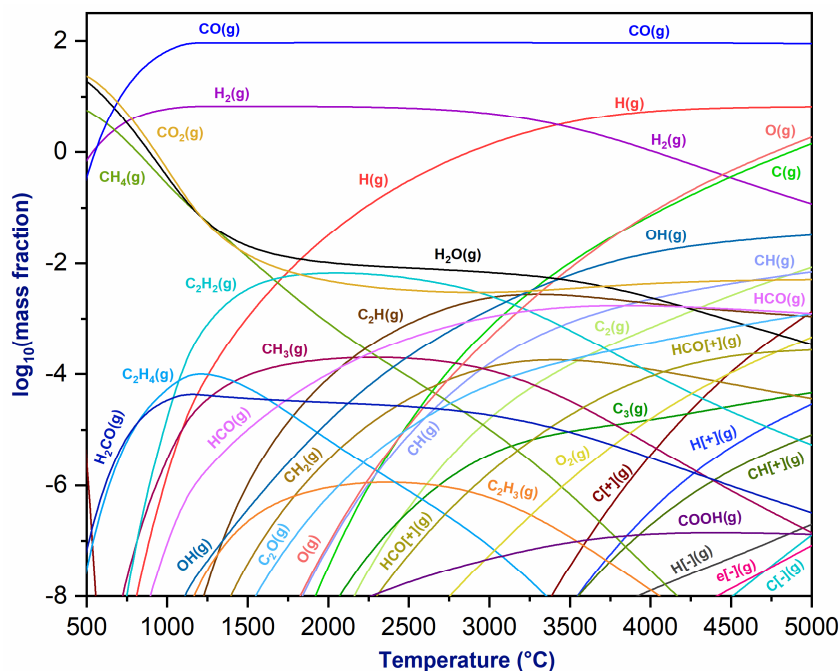


**Figure 3.** The variation of the mass fraction as a function of the temperature of the synthesized products for a mixed plasma  $\text{CO}_2/\text{CH}_4$  (molar ratio 1:1) at  $P = 1$  atm.

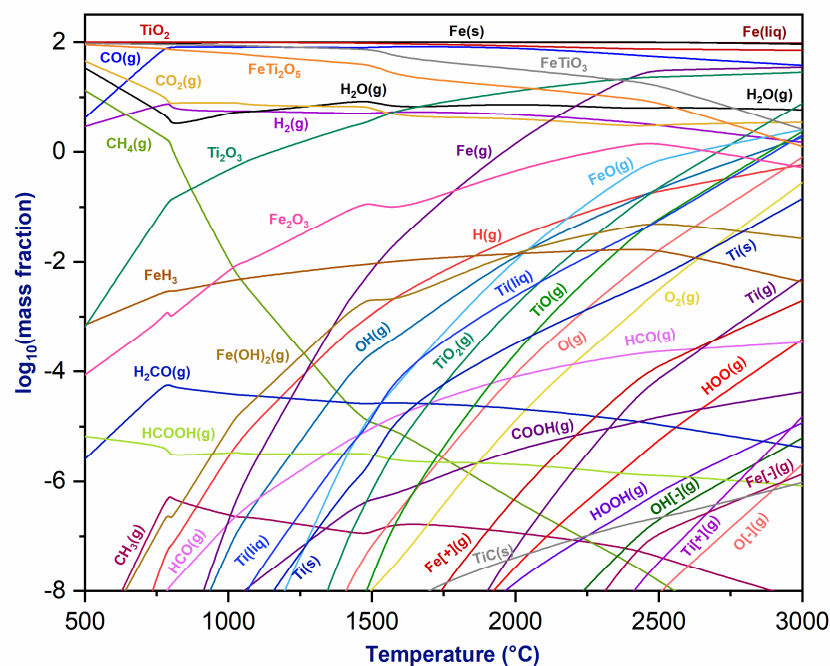


**Figure 4.** The variation of the mass fraction as a function of the temperature of the synthesized products for  $\text{CO}_2\text{-CH}_4$  plasma mixture (molar ratio: 1:1) and  $\text{FeTiO}_3$  system at  $P = 1$  atm.

### 3.1.2. CO<sub>2</sub>/CH<sub>4</sub> Molar Ratio 2:1

Depending on the operating conditions (temperature, pressure, and gas ratio), the reaction between CO<sub>2</sub> and CH<sub>4</sub> takes place in a complex way, which leads to the production of different chemical species (ions, electrons, radicals, molecules). At high temperatures, CO, H<sub>2</sub>, and H<sub>2</sub>O are the basic by-products of the reaction between CO<sub>2</sub> and CH<sub>4</sub>. Overall, the process of CO<sub>2</sub> and CH<sub>4</sub> interacting in a plasma mixture is complex and may result in the creation of a wide range of chemical species, making it an important area of research for elucidating plasma behavior and its potential applications in a wide range of fields [34]. CO<sub>2</sub> is an oxidizing gas that may help dissociate one of the two oxygen atoms into CO:



The carbon ions (C<sup>-</sup> and C<sup>+</sup>) were a byproduct of the CH<sub>4</sub> breakdown [35]. The log<sub>10</sub>(mass fraction) of the CO<sub>2</sub>/CH<sub>4</sub> plasma mixture (molar ratio 2:1) at equilibrium is shown as a function of temperature in Figure 5.

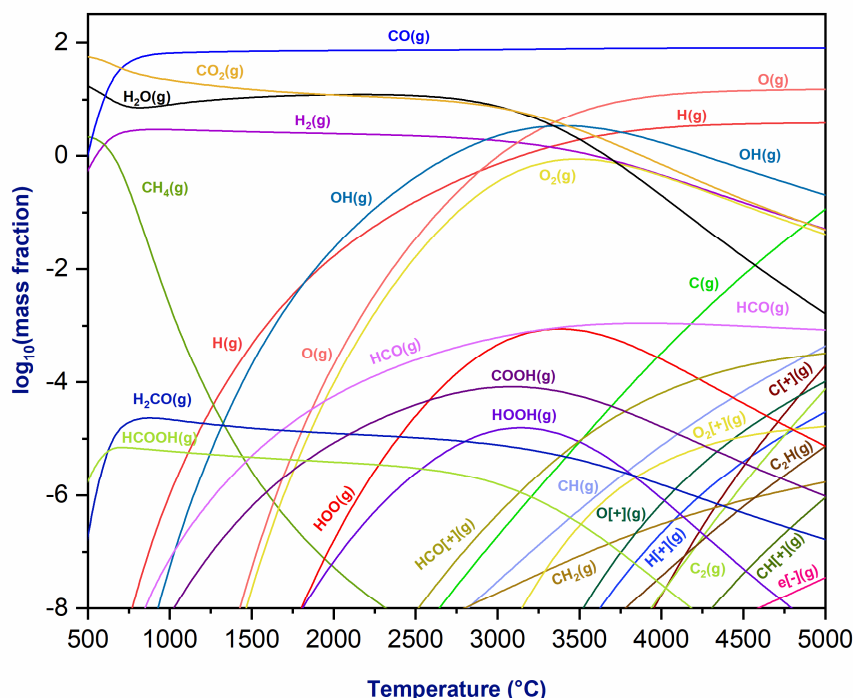


**Figure 5.** The variation of the mass fraction as a function of the temperature of the synthesized products for a mixed plasma CO<sub>2</sub>/CH<sub>4</sub> (molar ratio 2:1) at P = 1 atm.

Figure 6 shows the equilibrium log<sub>10</sub>(mass fraction) of the CO<sub>2</sub>/CH<sub>4</sub> plasma mixture and FeTiO<sub>3</sub> as a function of temperature. The production of iron metal Fe(s) starts above 500 °C and remains stable before producing Fe(liq). Similarly, TiO<sub>2</sub> is produced at this range. Likewise, the ilmenite (FeTiO<sub>3</sub>) phase is stable, and its mass fraction decreases by increasing the temperature, whereas Ti<sub>2</sub>O<sub>3</sub> and Fe<sub>2</sub>O<sub>3</sub> appear at low temperatures, and their mass fractions increase with increasing temperature. Moreover, Ti(s) and Ti(liq) are produced at over 900 °C, and their amounts increase until the temperature reaches 3000 °C. Fe(g) and Ti(g) originally evolved at temperatures of around 800 °C and 1700 °C, respectively.

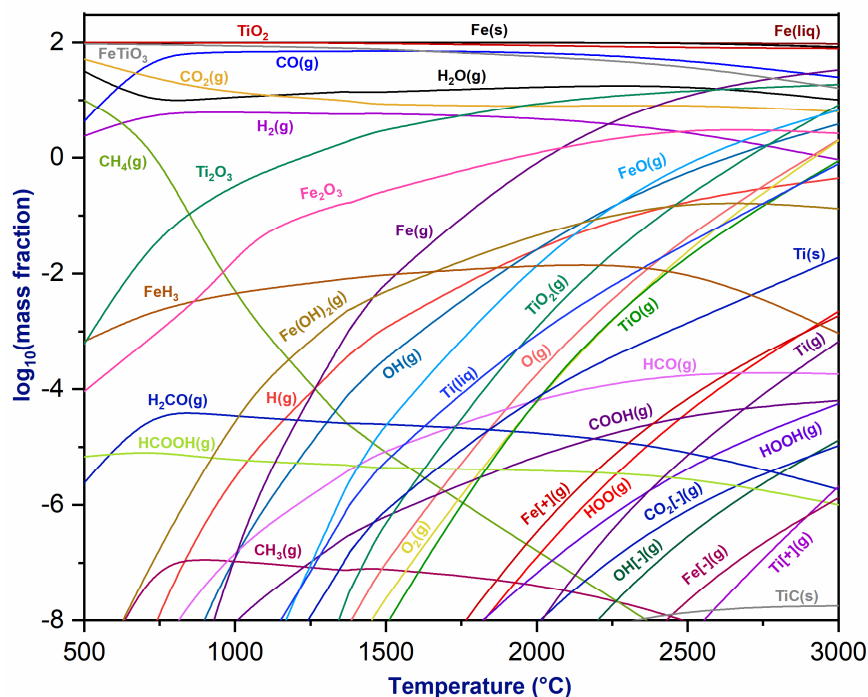


**Figure 6.** The variation of the mass fraction as a function of the temperature of the synthesized products for CO<sub>2</sub>-CH<sub>4</sub> plasma mixture (molar ratio: 2:1) and FeTiO<sub>3</sub> system at P = 1 atm.

### 3.2. Characteristics of the Plasma Jet

#### 3.2.1. Voltage-Current

The volt-ampere features of plasma torches are influenced by several factors, including cathode and anode materials, electrode structure size, working gas type, and flow rate. Voltage is the primary cause of free charge formation currently. To determine the parameter conditions for plasma treatment effect, the highest voltage discharge parameter must be determined [31]. Table 3 depicts the volt-ampere characteristics of the arc plasma torch used in this paper.

**Table 3.** Voltage-current characteristics of a plasma torch operating with CO<sub>2</sub> and CH<sub>4</sub>.

	Current (A)	Voltage (V)
Ratio 1:1	252	155
Ratio 2:1	252	150

Table 3 indicates that the current remains constant throughout the experiment; however, voltage changes until it reaches a level suitable for the formation of a stable plasma jet. The fluctuation of the voltage can be explained by the relationship between electrical resistance and power dissipation, i.e., the increase in electrical resistance is due to the rise in temperature and density generated by the current [20]. Figure 7 depicts the morphology of the plasma arc under the experiment’s stable conditions.

#### 3.2.2. Power Variation of CO<sub>2</sub>/CH<sub>4</sub> Molar Ratio

Gas plasma characteristics rely on a molar-gas ratio. Due to the varying proportions of these gases, a gas plasma combined with a 1:1 CO<sub>2</sub>/CH<sub>4</sub> molar ratio differs from a 2:1 molar ratio. As a result, the power of the 1:1 ratio is greater than that of the 2:1 ratio throughout the experiment. This is due to various parameters such as voltage, current, pressure, temperature, and material behavior. A plasma with a 1:1 CO<sub>2</sub>/CH<sub>4</sub> molar ratio may yield a hotter, more reactive plasma with a greater reactive species concentration than one with a 2:1 molar ratio. The stability and safe functioning of the plasma require constant

monitoring of the circumstances and the implementation of any required modifications [4]. Figure 8 illustrates the power variation over time in a spouted bed reactor.

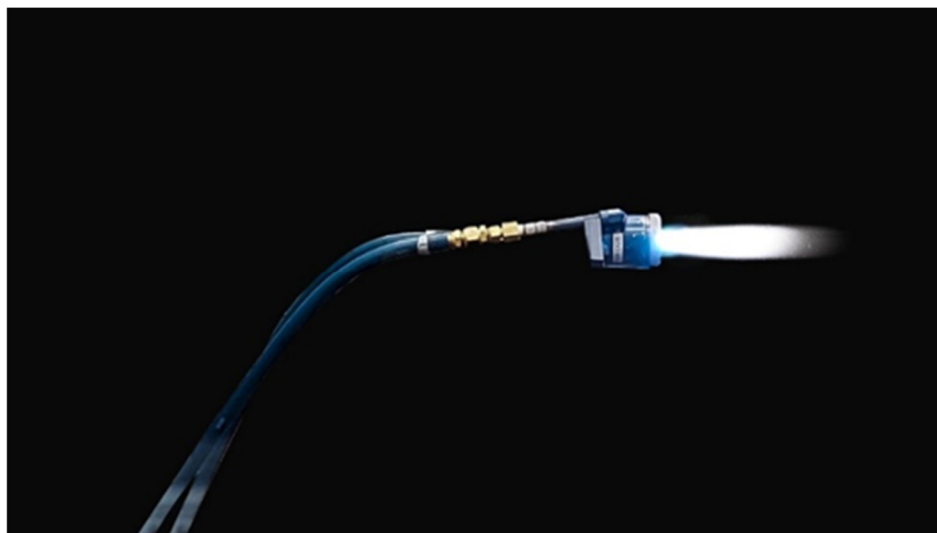


Figure 7. Image of the plasma jet.

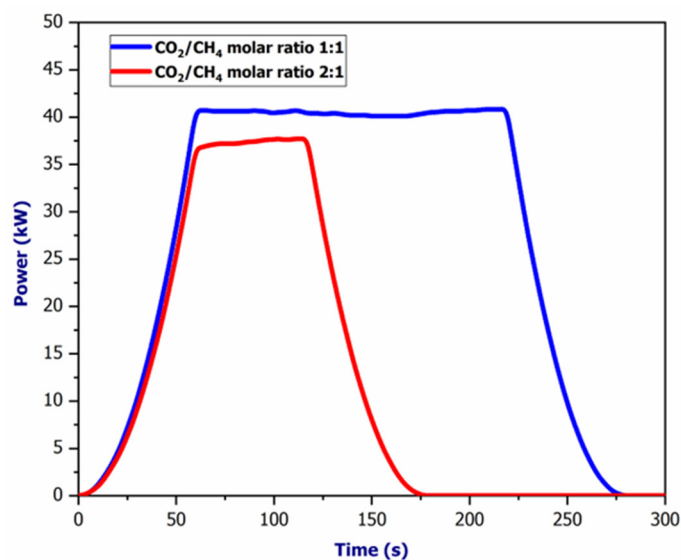


Figure 8. Power variation over time for CO<sub>2</sub>/CH<sub>4</sub> molar ratio of 1:1 and 2:1 at a current of 252 A.

### 3.2.3. Temperature Variation in Spouted Bed Reactor

The temperature inside the reactor bulk increases rapidly to reach more than 700 °C by using the CO<sub>2</sub>/CH<sub>4</sub> molar ratio of 1:1, and after that, it decreases after 500 s. As for the molar ratio of 2:1, it did not exceed 500 °C. Figure 9 shows the variation of the temperature as a function of time. The temperature variation is divided into two different parts: the heating part and the cooling part. The DC plasma torches working with a gas mixture of CO<sub>2</sub> and CH<sub>4</sub> generate high enthalpies (50 MJ/kg). The plasma enthalpy reveals a system's heat content. As a result, the thermodynamic property of the plasma arc is affected by particle density, plasma gases, and ionization degree [36]. As a result, the presence of a high electron density makes the environment more energetic and reactive, allowing the arc plasma to create a rich region for chemical species activation [37].

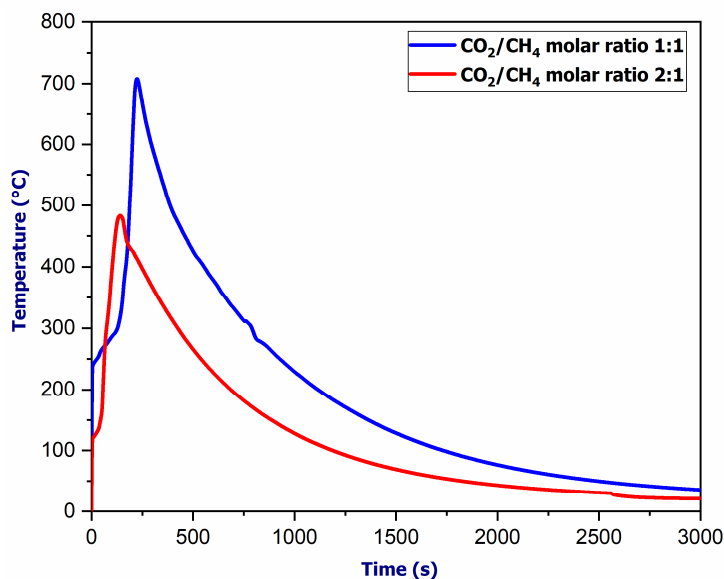


Figure 9. Temperature variation inside the spouted bed reactor.

A plasma jet was created at the torch output at the start of each experiment, coming into direct contact with the material that needed to be reduced. Temperatures above 3000 °C were obtained, melting the material and generating a liquid phase. This liquid phase was then cooled using an argon flow, resulting in a molten material known as the “solidified liquid phase,” which took on the same form as the reactor’s conical section. The process may be divided into three separate zones: the conical section, where the liquid phase solidifies to create a conical shape; the reactor walls, where the particles have stuck; and the particles floating in the air. Figure 10 depicts the various sections created in the conical portion around the plasma jet.

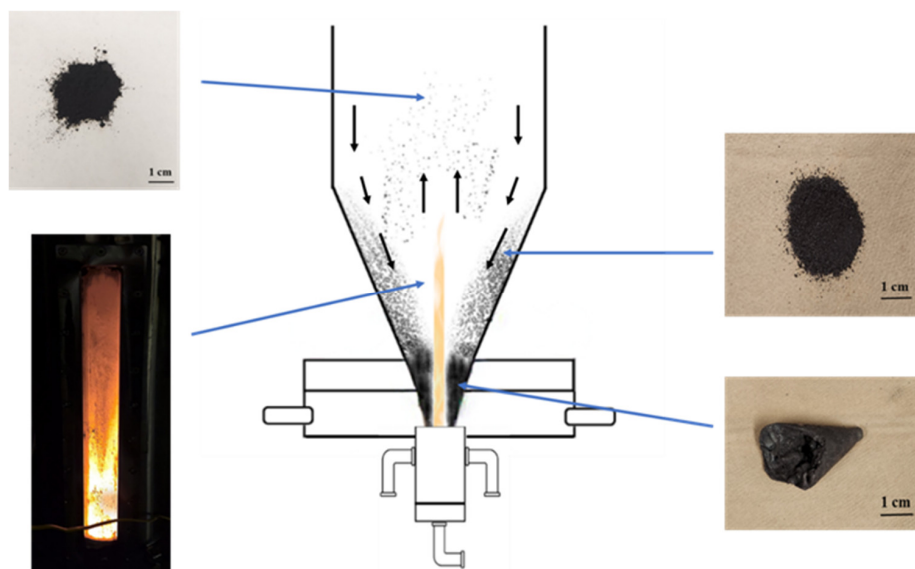


Figure 10. Schematic of a spouted bed.

### 3.3. Plasma Treatment of Natural Ilmenite Concentrate

#### 3.3.1. XRD Analysis

The X-ray diffractogram of feed material before and after thermal plasma treatment is shown in Figure 11. The primary constituents of the raw material are ilmenite (FeTiO<sub>3</sub>), magnetite (Fe<sub>3</sub>O<sub>4</sub>), titanium dioxide (TiO<sub>2</sub>), and sodium aluminum silicate (Na<sub>6</sub>Al<sub>6</sub>Si<sub>10</sub>O<sub>32</sub>).

Using a plasma torch working with CO<sub>2</sub> and CH<sub>4</sub>, ilmenite concentrate has been reduced to iron metal (Fe) and titanium (Ti), besides the ilmenite phase (FeTiO<sub>3</sub>) and iron oxide (FeO). The XRD patterns show that the ilmenite concentrate has been reduced using two molar ratios of 1:1 and 2:1, indicating that the CO<sub>2</sub>/CH<sub>4</sub> DC torch will be a novel and efficient technology in mineral processing and material extraction. As a result, the plasma treatment may separate titanium from iron metal, potentially increasing purification over traditional methods used in metallurgy extractives [38].

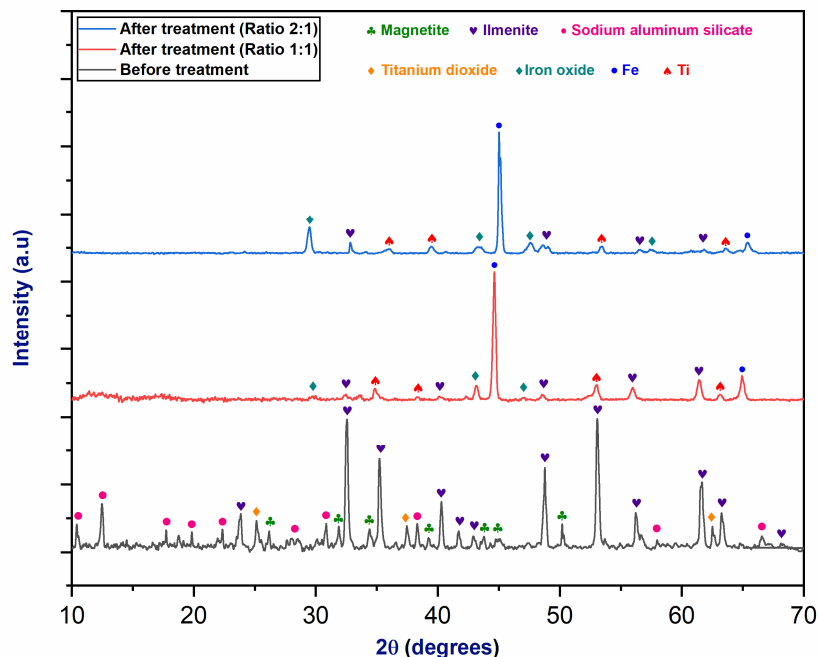


**Figure 11.** X-ray diffractogram of natural ilmenite before and after plasma treatment in the conical section.

Rietveld analysis was performed to determine the fraction of each crystalline phase before and after plasma treatment. X-ray diffraction (XRD) and Rietveld investigations demonstrated that the CO<sub>2</sub>/CH<sub>4</sub> plasma torch effectively reduced the ilmenite concentrate utilized in the trials, resulting in metals such as titanium and metallic iron. Crucially, the gas ratio is critical to reaching this purpose. The 1:1 molar ratio favored more titanium production over the 2:1 ratio, but the latter favored higher iron production. This finding may be related to the enhanced reactivity of CO<sub>2</sub> and CH<sub>4</sub>, which causes a rise in the CO/H<sub>2</sub> ratio in the reactor cone at higher temperatures, promoting an increase in the reduction [39]. Table 4 shows the Rietveld analysis of ilmenite concentrate before and after plasma treatment.

**Table 4.** Rietveld analysis of ilmenite concentrate before and after plasma treatment in the conical section.

Raw Material	Phase	Magnetite	Ilmenite	Titanium dioxide	Sodium aluminum silicate	
	wt% (±2)	5.3	78.7	3.1	12.9	
After treatment (ratio 1:1)	Phase	-	Ilmenite	Iron	Titanium	Iron oxide
	wt% (±2)	-	29.3	62.1	8.3	0.2
After treatment (ratio 2:1)	Phase	-	Ilmenite	Iron	Titanium	Iron oxide
	wt% (±2)	-	18.2	68.7	4.2	8.9

### 3.3.2. SEM-EDS Analysis

The SEM image of the ilmenite concentrate before and after plasma treatment is shown in Figure 12. As a result, the analysis reveals a clean and smooth surface of natural ilmenite concentrate before plasma treatment. However, after thermal treatment for both molar ratios (2:1 and 1:1), a melted surface was observed, resulting in two distinct regions (titanium area and iron area) [40]. Iron, titanium, oxygen, silicon, aluminum, and vanadium make up the bulk of the ilmenite concentrate, as shown in Figure 13, which displays the phase distribution of ilmenite prior to thermal treatment. Oxygen is found in high concentrations due to the existence of many oxides in raw materials like  $\text{TiO}_2$ . After plasma treatment, a phase composed entirely of titanium emerges, surrounded by a second metal phase composed of iron. Figures 14 and 15 show that the amount of oxygen has been reduced.

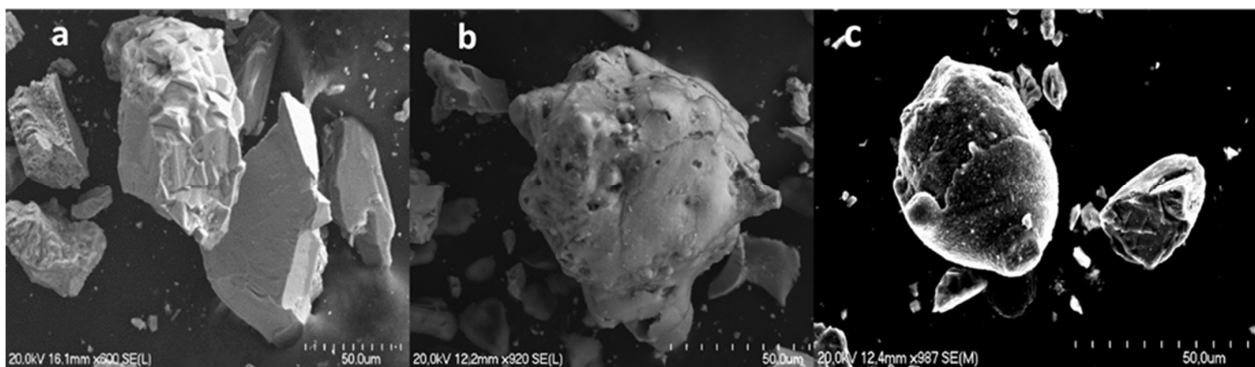


**Figure 12.** SEM image of ilmenite concentrate (a) before plasma treatment, (b) after plasma treatment (ratio 2:1), and (c) after plasma treatment (ratio 1:1) in the conical section.

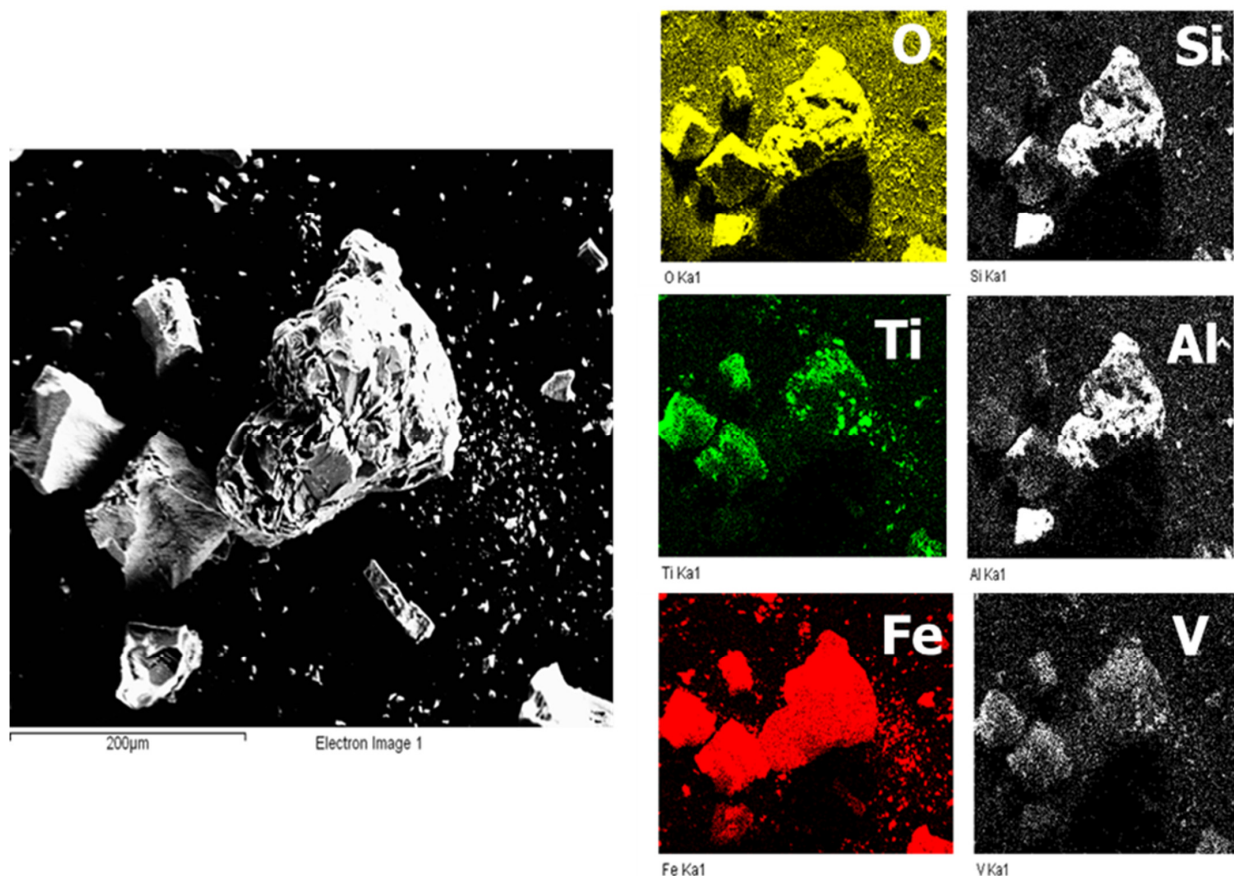


**Figure 13.** Morphology and elements distribution of ilmenite concentrate before plasma treatment.

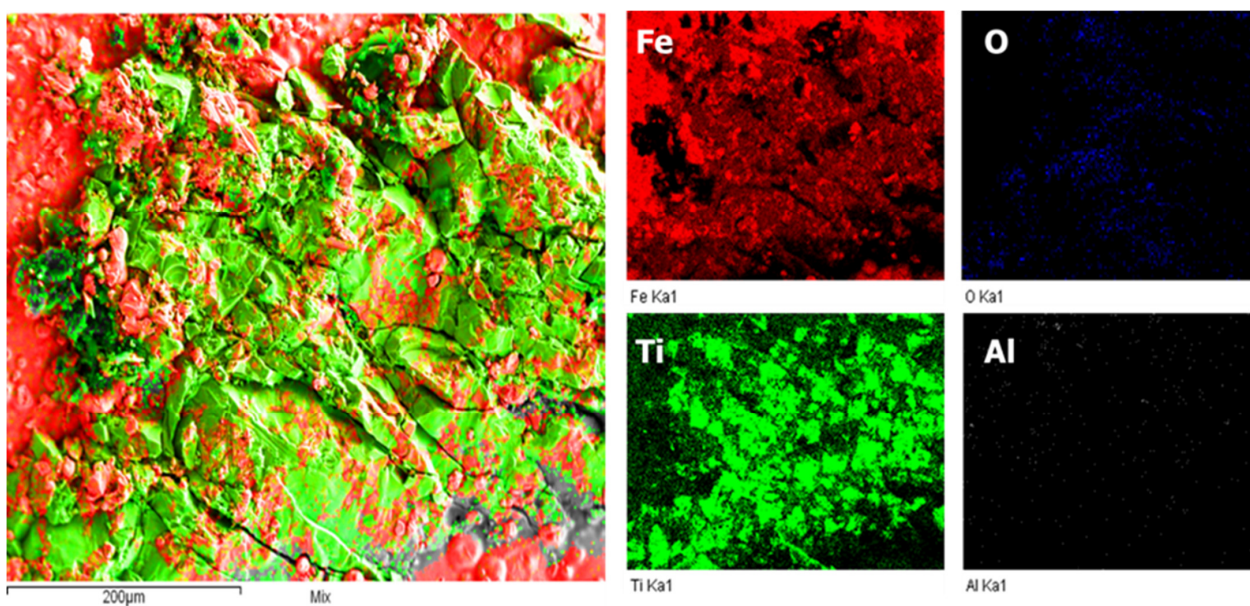


**Figure 14.** Morphology and elements distribution of ilmenite concentrate after plasma treatment using the 1:1 molar ratio in the conical section.

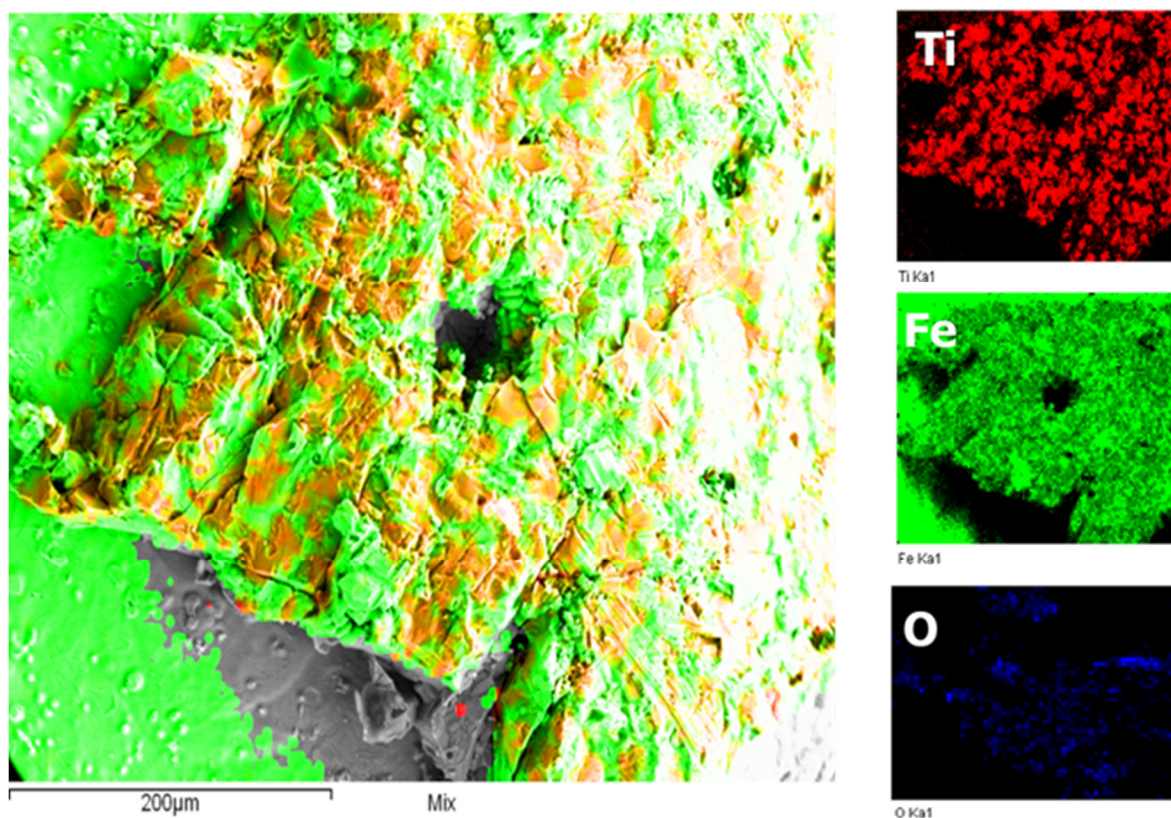
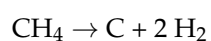


**Figure 15.** Morphology and elements distribution of ilmenite concentrate after plasma treatment using the 2:1 molar ratio in the conical section.

### 3.3.3. Outlet Gas Analysis

CO<sub>2</sub> and CH<sub>4</sub> reacted with each other in the plasma torch, which made a lot of other chemical species. The quantity of CH<sub>4</sub> decreases with rising temperature owing to the interactions of:





which results in the generation of oxidized carbon gases. A dissociation process occurred:



which causes the CO<sub>2</sub> level to decrease as the temperature within the plasma reactor increases [29]. As a result, the CH<sub>4</sub> quantity is critical, and increasing it causes the plasma torch to have more reduction power. It is important to note that the gases released would have a composition determined by the plasma, its reactions, and the desired outcomes. Depending on the conditions under which the plasma combination was created and the outcome of the reaction, other gases may be released. Figures 16 and 17 show the analysis of the partial pressure of output gases using both molar ratios 1:1 and 2:1, respectively. Thus, a 1:1 molar ratio promotes the formation of CO at the reactor exit, but a 2:1 ratio promotes the formation of both CO and H<sub>2</sub>. The fact that O<sub>2</sub> is not injected directly into the reactor implies that it comes in from the outside air. This observation is expected, considering that the reactor is not hermetically sealed and runs at pressures close to one atmosphere. It is important to note that the material was heated in an oven at 105 °C for 24 h before the experiment, which explains the low quantity of H<sub>2</sub>O. This demonstrates that plasma produces H<sub>2</sub>O. On the other hand, O<sub>2</sub> works as an oxidizer, converting CO to CO<sub>2</sub> and H<sub>2</sub> to H<sub>2</sub>O. This explains why the CO<sub>2</sub> levels are higher while the plasma is active.

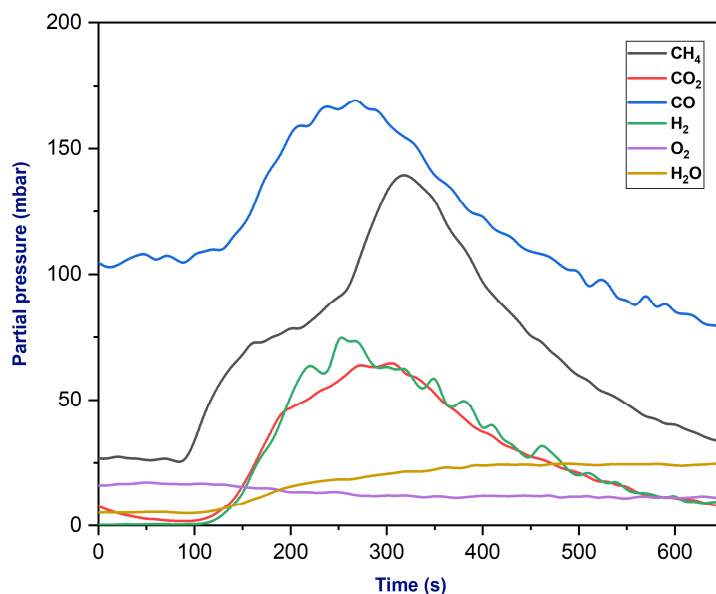


Figure 16. Analysis of the partial pressure of the output gas (molar ratio 1:1).

### 3.3.4. Mass Balance

The concept of mass balance states that a process’s inputs must equal its outputs. To achieve peak performance, a process must take into account both mass balance and process economics. Figure 18 highlights some pictures of the ilmenite concentration from various viewpoints.

Table 5 displays an 88% mass recovery for the molar ratio 1:1 and 77% for the ratio 2:1, demonstrating that the method minimizes waste and maximizes product recovery. In conclusion, maintaining a good mass balance is crucial to the success of the plasma process and the realization of its intended outcomes.

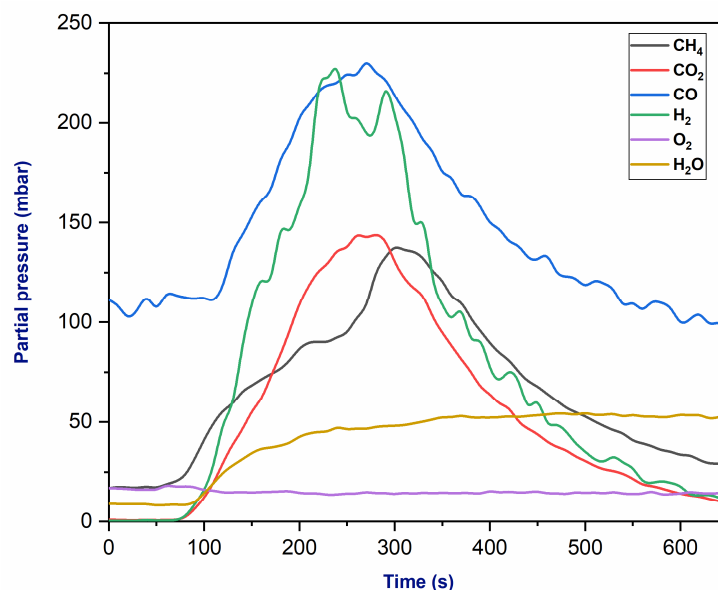


Figure 17. Analysis of the partial pressure of the output gas (molar ratio 2:1).

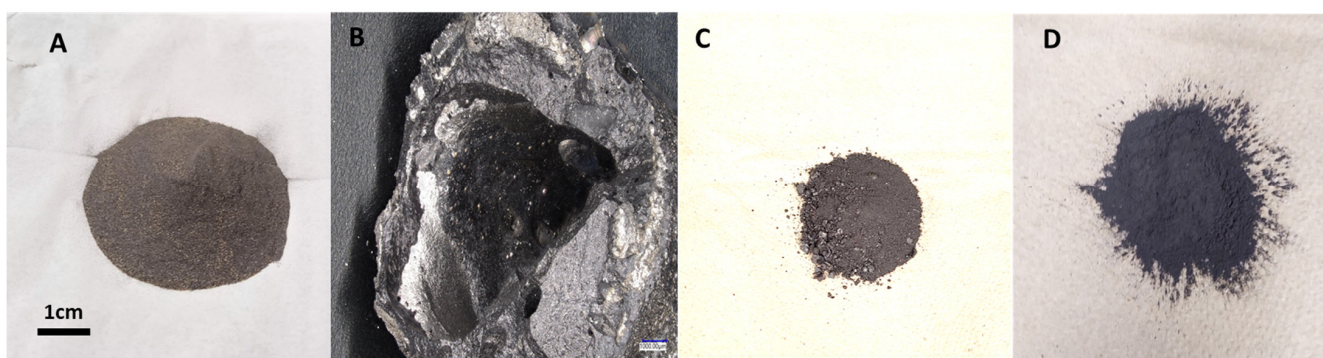


Figure 18. Image of ilmenite concentrates from different parts of the setup: (A) raw material; (B) cone part; (C) powder part; (D) filter part.

Table 5. Mass balance of the process.

Molar Ratio (CO <sub>2</sub> /CH <sub>4</sub> )	Raw Material (g)	Powder + Cone Part (g)	Filter Part (g)	Recovery (%)
1:1	250	214	6	88
2:1	250	175	18	77

### 3.3.5. Carbon Balance

The production of CO<sub>2</sub> must be taken into account to compensate for its impact on climate change and the global environment [41]. The monitoring of greenhouse gas emissions has become crucial to the protection of the environment. However, the carbon footprint can increasingly give a concrete idea of this kind of emission and control its activity. It enables us to identify the major emissions and initiate a reduction process for these emissions in a priority order [42]. Quantities of the various chemical compounds employed in this process using the molar ratio 1:1 and 2:1 are listed in Table 6.

**Table 6.** Comparing the input and output quantities of chemical species.

Species	Quantity (g)			
	Input		Output	
Molar ratio	1:1	2:1	1:1	2:1
FeTiO <sub>3</sub>	250	250	-	-
CO <sub>2</sub>	96.4	87.2	17.5	18.0
CH <sub>4</sub>	28.8	16.4	16.2	8.0
CO	-	-	28.6	23.8
H <sub>2</sub>	-	-	0.8	1.2
H <sub>2</sub> O	-	-	4.7	5.6

The following formulas show the CO<sub>2</sub> and CH<sub>4</sub> conversion calculations:

$$X(\text{CO}_2) = \frac{n_i(\text{CO}_2) - n_f(\text{CO}_2)}{n_i(\text{CO}_2)} \tag{7}$$

$$X(\text{CH}_4) = \frac{n_i(\text{CH}_4) - n_f(\text{CH}_4)}{n_i(\text{CH}_4)} \tag{8}$$

Here,  $n_i(\text{CO}_2)$  and  $n_f(\text{CO}_2)$  are the injected and the final mole number of CO<sub>2</sub>, respectively, and  $n_i(\text{CH}_4)$  and  $n_f(\text{CH}_4)$  are the injected and the final mole number of CH<sub>4</sub>, respectively.

According to the data in Figure 19, the conversion yield of CO<sub>2</sub> for this plasma process is approximately 80%. Otherwise, the conversion yield of CH<sub>4</sub> is approximately 55%.

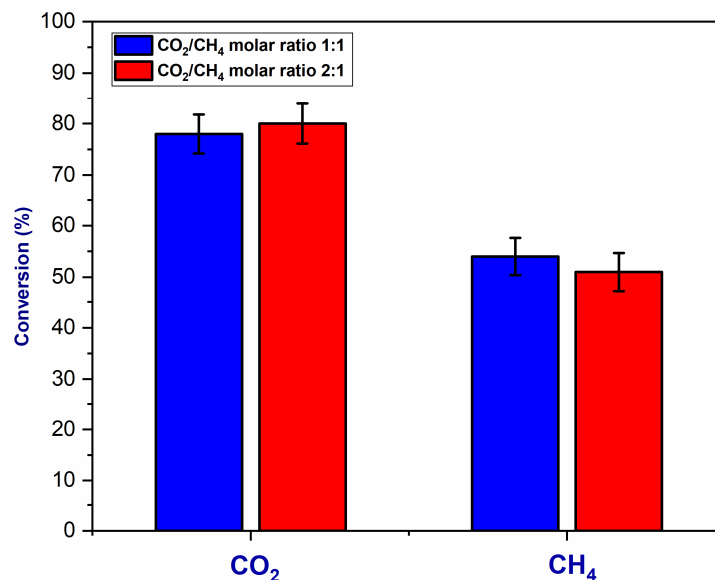


**Figure 19.** Conversion yield of CO<sub>2</sub> and CH<sub>4</sub>.

A carbon balance of one indicates that all of the reaction’s products have been adequately detected and quantified; on the other hand, a balance less than one can result from the adsorption of certain products formed, specifically carbon solid [43].

The following is the relationship used to calculate the carbon assessment:

$$\text{Carbon assessment} = \frac{(n(\text{CO}_2) + n(\text{CH}_4) + n(\text{CO}))}{n_i(\text{CO}_2) + n_i(\text{CH}_4)} \tag{9}$$

$$\begin{aligned} \text{Carbon assessment}(1 : 1) &= 0.62 \\ \text{Carbon assessment}(2 : 1) &= 0.58 \end{aligned} \quad (10)$$

The “ideal” carbon balance for a process involving ilmenite, CO<sub>2</sub>, and CH<sub>4</sub> may be either positive (indicating a surplus) or negative (indicating a deficit). A positive carbon balance suggests that carbon-containing molecules are being produced on the net, which may be advantageous if their creation is the ultimate aim. A positive carbon balance is required to produce TiC if the latter is the final product required. As well, the reduction of the amount of carbon to form CO<sub>2</sub> and H<sub>2</sub>O from the starting products results in a negative carbon balance. In conclusion, the intended end products will affect the conception of the balance and determine whether a positive or negative carbon balance is achieved. It should be noted that a carbon assessment is only one type of assessment that can be performed in a plasma reaction, and that other assessments (such as a hydrogen balance or an elemental balance) may also be needed to fully characterize the reaction, depending on the specific system and desired end products [44].

### 3.4. Economic Study

#### 3.4.1. CAPEX (Capital Expenditures)

The economic analysis was conducted to emphasize the expenses of the pilot procedure. A cost analysis must be performed concurrently to assure the accuracy of the economic data provided [45]. In order to provide a more reasonable evaluation, overall equipment costs were determined using factorial analysis based on the major delivered-equipment cost for a solid-liquid process [46]. The goal of this method is to get a thorough knowledge of the necessary investments, taking into consideration a variety of aspects related to the equipment used in the process [47]. Table 7 shows the total estimated cost of capital investment.

**Table 7.** Estimate cost of the total capital investment (TCI).

	Cost (US\$)
Total plasma equipment	465,546
Total direct plant cost	1,620,100
Total direct + indirect plant cost	1,927,360
Fixed capital investment (FCI)	2,178,755
Working capital	344,504
Total capital investment (TCI)	2,523,259

#### 3.4.2. OPEX (Operating Expenditures)

Scaling up is essentially the reduction of investment through the development of large-scale processes that can scale up volumetrically. This scaling is generally based on relationships between installed equipment cost and investment, so different pieces of equipment assign scaling factors to each other [48]. Numbering up assumes that laboratory-scale equipment can be used on a large scale (industrial scale) and does not need to be larger. It was conducted an OPEX study in which all operating expenses were calculated [49]. The process for determining the after-tax net cash flow year after year employs a marginal tax rate of 40% based on the Canadian income tax system. We estimate a 40% salvage value for equipment and building after 10 years. The tax depreciation rates used are a constant decreasing rate of 4% for category 1 buildings and 50% for category 53 equipment. The total cost of operating expenses is shown in Table 8.

Table 8. The estimated total cost of expenses.

<b>Income Statement</b>												
<b>Year</b>	0	1	2	3	4	5	6	7	8	9	10	
<b>Revenues</b>	0	0	0	0	0	0	0	0	0	0	0	
<b>Expenses (US\$/year)</b>												
Operating cost		316,010	316,010	316,010	316,010	316,010	316,010	316,010	316,010	316,010	316,010	
Services and utilities		210,766	210,766	210,766	210,766	210,766	210,766	210,766	210,766	210,766	210,766	
Fixed charges		30,503	30,503	30,503	30,503	30,503	30,503	30,503	30,503	30,503	30,503	
Plant overhead costs		125,327	125,327	125,327	125,327	125,327	125,327	125,327	125,327	125,327	125,327	
Administrative expenses		15,666	15,666	15,666	15,666	15,666	15,666	15,666	15,666	15,666	15,666	
Depreciation												
Buildings		931	1825	1752	1682	1615	1550	1488	1428	1371	1316	
Equipment		533,050	799,575	399,788	199,894	99,947	49,973	24,987	12,493	6247	3123	
<b>Taxable income</b>		−1,232,254	−1,499,673	−1,099,812	−899,848	−799,834	−749,796	−724,747	−712,194	−705,890	−702,712	
<b>Income taxes</b>		−492,901	−599,869	−439,925	−359,939	−319,934	−299,918	−289,899	−284,878	−282,356	−281,085	
<b>Net income</b>		−739,352	−899,804	−659,887	−539,909	−479,900	−449,878	−434,848	−427,317	−423,534	−421,627	
<b>Cash flow statement</b>												
<b>Operating activities</b>												
Net income		−739,352	−899,804	−659,887	−539,909	−479,900	−449,878	−434,848	−427,317	−423,534	−421,627	
Depreciation		533,981	801,400	401,540	201,576	101,561	51,523	26,475	13,922	7618	4440	
<b>Investment activities</b>												
Buildings		−46,555									18,622	
Equipment		−2,132,201									852,880	
Disposal tax adjustment											−334,713	
<b>Net cash flow</b>		−2,178,755	−205,371	−98,403	−258,348	−338,333	−378,339	−398,354	−408,374	−413,395	−415,916	119,601

#### 4. Conclusions

In several domains, looking for tools that offer low cost and high productivity has become critical. Plasma technology is one of those tools that has been developed for a variety of applications, particularly in material processing. A novel DC CO<sub>2</sub>/CH<sub>4</sub> plasma torch was used in this study to reduce an ilmenite concentrate. Overall, the reduction of ilmenite concentrate by a reducing plasma torch is the result of a series of thermal and chemical processes that result in the minimization of oxygen in the cone part of the plasma reactor while isolating the titanium and iron components. In addition, the effect of the CO<sub>2</sub>/CH<sub>4</sub> molar ratio was studied, and it was observed that a 1:1 ratio could generate higher temperatures and power inside the reactor than a 2:1 ratio, leading to a more efficient reduction of the ilmenite concentrate. The XRD results show that plasma treatment can successfully be used to reduce the ilmenite concentrate and produce titanium and iron metal. As a result, SEM-EDS results highlight the separation of titanium and iron in some areas, emphasizing an important benefit of using plasma treatment. Furthermore, a thermodynamic study was provided to predict the appearance of thermodynamically stable phases. To focus on the next step to further develop the process, an OPEX and CAPEX study were provided for a process scale-up study. No revenue was introduced into this study because titanium commercial-grade quality was not determined, as this stage was first initiated as proof of concept, which was done. More reliable data will be obtained during the process scale-up. As a result, thermal plasma treatment was used in this study and demonstrated excellent metallurgy extractive performance. To achieve the required reaction and highly pure products, it is essential to precisely regulate the plasma reduction process's operating parameters, such as gas flow rate, temperature, and plasma energy. In terms of plasma gases, mass spectrometry analysis and thermodynamic calculations have proven that CH<sub>4</sub> and CO<sub>2</sub> decompose into H<sub>2</sub> and CO. This process will reduce the environmental impact associated with the thermal treatment of ilmenite by consuming greenhouse gases instead of producing them. In the near future, an optimized reactor will be developed to scale up the technology at the pilot stage. This exciting development will greatly increase operating performance in extreme conditions. The economic implications of this new technology will be thoroughly investigated, with a focus on its beneficial influence on revenue and profitability.

**Author Contributions:** Conceptualization, M.E.K. and G.S.; formal analysis, M.E.K.; funding acquisition, G.S., J.L. and M.P.; investigation, M.E.K.; methodology, M.E.K.; resources, G.S., J.L., and M.P.; supervision, G.S.; validation, M.E.K.; writing—original draft preparation, M.E.K.; writing—review and editing, M.E.K., G.S., J.L. and M.P. All authors have read and agreed to the published version of the manuscript.

**Funding:** This study was funded by NSERC (Natural Sciences and Engineering Research Council of Canada) discovery grant (RGPIN-2018-06128) and Metchib company-Quebec, Canada.

**Data Availability Statement:** Data are contained within the article.

**Acknowledgments:** Metchib Company sponsored this study. We appreciate Metchib Company in Canada for giving us ilmenite concentrate samples and helping us.

**Conflicts of Interest:** Jonathan Lapointe and Mathieu Paquet were employed by the company Resources Metchib Inc. The remaining authors declare that the research was conducted in the absence of any commercial or financial relationships that could be construed as a potential conflict of interest.

#### References

1. Samal, S.; Blanco, I. An Overview of Thermal Plasma Arc Systems for Treatment of Various Wastes in Recovery of Metals. *Materials* **2022**, *15*, 683. [[CrossRef](#)] [[PubMed](#)]
2. Samal, S. *Thermal Plasma Processing of Materials: High Temperature Applications*; Elsevier: Amsterdam, The Netherlands, 2020.
3. Gautier, M.; Rohani, V.; Fulcheri, L. Direct decarbonization of methane by thermal plasma for the production of hydrogen and high value-added carbon black. *Int. J. Hydrogen Energy* **2017**, *42*, 28140–28156. [[CrossRef](#)]
4. Samal, S. Thermal plasma technology: The prospective future in material processing. *J. Clean. Prod.* **2017**, *142*, 3131–3150. [[CrossRef](#)]

5. El Khalloufi, M.; Drevelle, O.; Soucy, G. Titanium: An Overview of Resources and Production Methods. *Minerals* **2021**, *11*, 1425. [[CrossRef](#)]
6. Jin, T.; Costa, M.; Chen, X. Chapter 34—Titanium. In *Handbook on the Toxicology of Metals*, 5th ed.; Nordberg, G.F., Costa, M., Eds.; Academic Press: Cambridge, MA, USA, 2022.
7. Rezaei Ardani, M.; Sheikh Abdul Hamid, S.A.R.; Mohamed, A.R. Synthesis of TiH<sub>2</sub> powder from ilmenite using MgH<sub>2</sub> under H<sub>2</sub> atmosphere. *Mater. Lett.* **2021**, *298*, 129997. [[CrossRef](#)]
8. Jena, K.D.; Xu, S.; Hayat, M.D.; Zhang, W.; Cao, P. Aiming at low-oxygen titanium powder: A review. *Powder Technol.* **2021**, *394*, 1195–1217. [[CrossRef](#)]
9. Earlam, M.R. Chapter 6—The Kroll process and production of titanium sponge. In *Extractive Metallurgy of Titanium*; Fang, Z.Z., Froes, F.H., Zhang, Y., Eds.; Elsevier: Amsterdam, The Netherlands, 2020.
10. Okabe, T.H.; Takeda, O. Chapter 5—Fundamentals of thermochemical reduction of TiCl<sub>4</sub>. In *Extractive Metallurgy of Titanium*; Fang, Z.Z., Froes, F.H., Zhang, Y., Eds.; Elsevier: Amsterdam, The Netherlands, 2020.
11. Matviychuk, M.; Klevtsov, A.; Moxson, V.S. Chapter 7—A modified Kroll process via production of TiH<sub>2</sub>—Thermochemical reduction of TiCl<sub>4</sub> using hydrogen and Mg. In *Extractive Metallurgy of Titanium*; Fang, Z.Z., Froes, F.H., Zhang, Y., Eds.; Elsevier: Amsterdam, The Netherlands, 2020.
12. Suzuki, R.O.; Natsui, S.; Kikuchi, T. Chapter 12—OS process: Calciothermic reduction of TiO<sub>2</sub> via CaO electrolysis in molten CaCl<sub>2</sub>. In *Extractive Metallurgy of Titanium*; Fang, Z.Z., Froes, F.H., Zhang, Y., Eds.; Elsevier: Amsterdam, The Netherlands, 2020.
13. Chen, G.Z.; Fray, D.J. Chapter 11—Invention and fundamentals of the FFC Cambridge Process. In *Extractive Metallurgy of Titanium*; Fang, Z.Z., Froes, F.H., Zhang, Y., Eds.; Elsevier: Amsterdam, The Netherlands, 2020.
14. Withers, J.C. Chapter 14—Electrolysis of carbothermic treated titanium oxides to produce Ti metal. In *Extractive Metallurgy of Titanium*; Fang, Z.Z., Froes, F.H., Zhang, Y., Eds.; Elsevier: Amsterdam, The Netherlands, 2020.
15. Taylor, P.R.; Manrique, M.; Pirzada, S.A.; Abdel-Latif, M. Formation of Titanium Carbide from Ilmenite Concentrates in a Thermal Plasma Reactor. *Plasma Chem. Plasma Process.* **1995**, *15*, 545–557. [[CrossRef](#)]
16. Manrique, M.; Figueira, T.; Gómez, J.; Taylor, P.R. Thermal decomposition of ilmenite in a non-transferred arc thermal plasma flow reactor. *Astrophys. Space Sci.* **1997**, *256*, 499–503. [[CrossRef](#)]
17. Samal, S.; Mukherjee, P.S.; Ray, A.K. Comparative Study on Energy Consumption and Yield by Various Thermal Plasma Routes for Production of Titania slag. *Plasma Chem. Plasma Process.* **2010**, *30*, 413–428. [[CrossRef](#)]
18. Samal, S. Synthesis of TiO<sub>2</sub> Nanoparticles from Ilmenite Through the Mechanism of Vapor-Phase Reaction Process by Thermal Plasma Technology. *J. Mater. Eng. Perform.* **2018**, *27*, 2622–2628. [[CrossRef](#)]
19. Twarog, P.J.; Hackett, C.M.; Cook, D.J.; Altobelli, B.P.; Bouthillier, D.L. Plasma Arc Torch Having an Electrode with Internal Passages. U.S. Patent 8,680,425, 25 March 2014.
20. Pershin, L.; Mitrasinovic, A.; Mostaghimi, J. Treatment of refractory powders by a novel, high enthalpy dc plasma. *J. Phys. D Appl. Phys.* **2013**, *46*, 224019. [[CrossRef](#)]
21. Pershin, V.; Mostaghimi, J.; Chen, L. Highly Ordered Structure Pyrolytic Graphite or Carbon-Carbon Composite Cathodes for Plasma Generation in Carbon Containing Gases. U.S. Patent 8,642,917, 4 February 2014.
22. Mitrasinovic, A.; Pershin, L.; Mostaghimi, J. *Electronic Waste Treatment by High Enthalpy Plasma Jet*; International Plasma Chemistry Society (IPCS20): Philadelphia, PA, USA, 2013.
23. León-Reina, L.; García-Maté, M.; Álvarez-Pinazo, G.; Santacruz, I.; Vallcorba, O.; De la Torre, A.G.; Aranda, M.A.G. Accuracy in Rietveld quantitative phase analysis: A comparative study of strictly monochromatic Mo and Cu radiations. *J. Appl. Crystallogr.* **2016**, *49*, 722–735. [[CrossRef](#)] [[PubMed](#)]
24. McCusker, L.B.; Von Dreele, R.B.; Cox, D.E.; Louër, D.; Scardi, P. Rietveld refinement guidelines. *J. Appl. Crystallogr.* **1999**, *32*, 36–50. [[CrossRef](#)]
25. Lantagne, G.; Marcos, B.; Cayrol, B. Computation of complex equilibria by nonlinear optimization. *Comput. Chem. Eng.* **1988**, *12*, 589–599. [[CrossRef](#)]
26. Laflamme, C. *Production de Composés Aromatiques Liquides à Partir du Gaz Naturel, Utilisant un Réacteur à Plasma*; Memoire de Maitrise es Sciences Appliquees; Universite de Sherbrooke: Sherbrooke, QC, Canada, 1988.
27. Safa, S.; Soucy, G. Application of a Novel CO<sub>2</sub> DC Thermal Plasma Torch Submerged in Aqueous Solution for Treatment of Dissolved Carboxylic Acid. *Plasma Chem. Plasma Process.* **2015**, *35*, 21–43. [[CrossRef](#)]
28. Zhou, Y.; Chu, R.; Fan, L.; Zhao, J.; Li, W.; Jiang, X.; Meng, X.; Li, Y.; Yu, S.; Wan, Y. Conversion mechanism of thermal plasma-enhanced CH<sub>4</sub>-CO<sub>2</sub> reforming system to syngas under the non-catalytic conditions. *Sci. Total Environ.* **2023**, *866*, 161453. [[CrossRef](#)]
29. Safa, S.; Hekmat-Ardakan, A.; Soucy, G. Experimental and thermodynamic comparison between a novel CO<sub>2</sub>/CH<sub>4</sub> and an oxygen submerged DC thermal plasma for treatment of sebacic acid in basic aqueous solution. *J. Environ. Chem. Eng.* **2014**, *2*, 2136–2147. [[CrossRef](#)]
30. Czernichowski, A.; Czernichowski, M.; Wesolowska, K. GlidArc-assisted production of Synthesis Gas from Biogas. In Proceedings of the 1st European Hydrogen Energy Conference, Grenoble, France, 2–5 September 2003; pp. 2–5.
31. Yue, C.; Zhe, Y.; Jinmao, L.; Chunlian, S.; Zhihao, Z.; Dandan, L.; Xiaofang, Z. Study on purification of flaky graphite by argon arc plasma torch. *Intense Laser Part. Beams* **2021**, *33*, 065021.

32. Yunos, N.F.M.; Idris, M.A.; Nasrun, N.A.; Kurniawan, A.; Nomura, T.; Rezan, S.A. Structural Characterizations and Phase Transition on the Reducibility of Ilmenite Ore with Different Carbon Reductants by Carbothermal Reduction Under Hydrogen Atmosphere. *J. Sustain. Metall.* **2023**, *9*, 1716–1731. [[CrossRef](#)]
33. Xiao, W.; Lu, X.-G.; Zou, X.-L.; Li, C.-H.; Ding, W.-Z. Multiple gaseous reduction of ilmenite: Thermodynamic and experimental study. *Rare Met.* **2015**, *34*, 888–894. [[CrossRef](#)]
34. Lesueur, H.; Czernichowski, A.; Chapelle, J. Résumé: On étudie la production du gaz de synthèse (CO + H<sub>2</sub>) à partir de l'oxydation de CH<sub>4</sub> par CO<sub>2</sub> dans un électro-réacteur à décharges glissantes. *J. Phys. Colloq.* **1990**, *51*, 49. [[CrossRef](#)]
35. Safa, S.; Soucy, G. Decomposition of high molecular weight carboxylic acid in aqueous solution by submerged thermal plasma. *Chem. Eng. J.* **2014**, *244*, 178–187. [[CrossRef](#)]
36. Boulos, M.I.; Fauchais, P.; Pfender, E. *Thermal Plasmas: Fundamentals and Applications*; Plenum Press: New York, NY, USA, 1994.
37. Pershin, L.; Chen, L.; Mostaghimi, J. Comparison of molecular and argon gases for plasma spraying. In *Thermal Spray 2007: Global Coating Solutions*; ASM International: Materials Park, OH, USA, 2007; pp. 266–269.
38. Fang, Z.Z.; Paramore, J.D.; Sun, P.; Chandran, K.R.; Zhang, Y.; Xia, Y.; Cao, F.; Koopman, M.; Free, M. Powder metallurgy of titanium—past, present, and future. *Int. Mater. Rev.* **2018**, *63*, 407–459. [[CrossRef](#)]
39. Saghafi, M.H.; Kazemi, A.; Sanaei, A.; Rasti, A.; Arabi, S.H. Investigation on the pre-reduction of ilmenite pellet using H<sub>2</sub>/CO atmospheres. *Can. Metall. Q.* **2023**, *1*–9. [[CrossRef](#)]
40. Zhang, G.; Gou, H.; Wu, K.; Chou, K. Carbothermic reduction of Panzhihua ilmenite in vacuum. *Vacuum* **2017**, *143*, 199–208. [[CrossRef](#)]
41. Hammoud, D. Synthèses et Caractérisations D'oxydes Mixtes à Base de Cuivre, Zinc Et Aluminium Issus de Précurseurs de Type Hydrotalcite: Application Pour la Réaction de Vaporeformage du Biométhanol. Ph.D. Thesis, Université du Littoral côté d'Opal, Boulogne-sur-Mer, France, 2015.
42. Amoes. Bilan Carbone de la Société Amoes. 2017. Available online: <https://www.amoes.com/media/societe/impact-carbone/bilan-carbone-amoes-2017.pdf> (accessed on 20 April 2024).
43. Mrad, M.; Hammoud, D.; Gennequin, C.; Aboukaïs, A.; Abi-Aad, E. A comparative study on the effect of Zn addition to Cu/Ce and Cu/Ce–Al catalysts in the steam reforming of methanol. *Appl. Catal. A Gen.* **2014**, *471*, 84–90. [[CrossRef](#)]
44. Diab, J.; Fulcheri, L.; Hessel, V.; Rohani, V.; Frenklach, M. Why turquoise hydrogen will be a game changer for the energy transition. *Int. J. Hydrogen Energy* **2022**, *47*, 25831–25848. [[CrossRef](#)]
45. Sartori, D.; Catalano, G.; Genco, M.; Pancotti, C.; Sirtori, E.; Vignetti, S.; Del Bo, C. Guide to cost-benefit analysis of investment projects. In *Economic Appraisal Tool for Cohesion Policy 2014*; Department of Economics, Management and Quantitative Methods, University of Milan: Milan, Italy, 2020.
46. Maćzka, T.; Pawlak-Kruczek, H.; Niedzwiecki, L.; Ziaja, E.; Chorążyczewski, A. Plasma Assisted Combustion as a Cost-Effective Way for Balancing of Intermittent Sources: Techno-Economic Assessment for 200 MWel Power Unit. *Energies* **2020**, *13*, 5056. [[CrossRef](#)]
47. Peters, M.S.a.T.K.D. *Plant Design and Economics for Chemical Engineers*; McGraw-Hill: New York, NY, USA, 1991; p. 183.
48. Shin, H.; Kim, J.; Kim, J. Feasibility study on the recovery for valuable minerals in beach sand. *J. Korean Soc. Miner. Energy Resour. Eng.* **2013**, *50*, 534–542. [[CrossRef](#)]
49. Park, C.S. *Contemporary Engineering Economics*; Addison-Wesley: Boston, MA, USA, 1993; p. 469.

**Disclaimer/Publisher's Note:** The statements, opinions and data contained in all publications are solely those of the individual author(s) and contributor(s) and not of MDPI and/or the editor(s). MDPI and/or the editor(s) disclaim responsibility for any injury to people or property resulting from any ideas, methods, instructions or products referred to in the content.